JOURNAL OF MATERIALS SCIENCE 26 (1991) 3533–3543

Creep behaviour of Cu–30% Zn at intermediate temperatures

S. V. RAJ
NASA Lewis Research Center, MS 49-1, 21000 Brookpark Road, Cleveland, Ohio 44135, USA

The creep properties of single-phase Cu–30% Zn alpha brass were investigated in the intermediate temperature range 573–823 K (0.48–0.70 T_m, where T_m is the absolute melting point). Inverse, linear, and sigmoidal primary creep transients were usually observed above 573 K under stresses resulting in minimum creep rates between 10^{-7} and $2 \times 10^{-4} s^{-1}$, while normal primary creep occurred under all other conditions. The creep stress exponent decreased from about 5.4 at 573 K to about 4.1 above 623 K, and the activation energy for creep varied between 170 and 180 kJ mol^{-1}. A detailed analysis of the data, as well as a review of the literature, suggests that no clearly defined class M to class A to class M transition exists in this alloy, although the characteristics of both class A and class M behaviour are observed under nominally similar stresses and temperatures. It is concluded that Cu–30% Zn does not conform to the normally accepted characterization of class A or class M solid solution alloys.

1. Introduction

Depending on stress, σ, absolute temperature, T, and composition, many solid solution alloys exhibit either class A (alloy type) or class M (or metal type) creep behaviour each with its own distinguishable characteristic [1–4]. In general, the class M response results from a dislocation climb-controlled process leading to a stress exponent, n, of about 4.5, while class A behaviour is due to a viscous glide mechanism for which $n \approx 3$. Although this difference in the values of n is often used to identify creep mechanisms, it is important to note that such inferences can sometimes be erroneous. For example, n can equal ~ 3 for data obtained in the transition region between power-law and diffusion creep. Additionally, some solid solution alloys, such as Cu–30% Zn (wt % except as noted) [5, 6], Cu–16 (at %) Al [7] and Fe–1.8 (at %) Mo [8], often exhibit sigmoidal and inverse primary creep transients that are characteristic of class A response although values of $n \approx 4.5$ were reported in these investigations. Further confirmation of the dangers involved in identifying creep mechanisms solely on the basis of the magnitude of n is demonstrated by the recent observations of class M to class A to class M transitions in dilute Fe–Mo ($0.5 \leq$ Mo ≤ 2 at %) alloys [9, 10].

In view of the above observations on the Fe–Mo system, a re-examination of the creep behaviour of Cu–30% Zn is in order because it exhibits similar characteristics to the dilute Fe–Mo alloys. Table I gives the creep results on the nominally Cu–30% Zn single-phase alloy reported in several investigations [5, 6, 11–16]. Although Cu–30% Zn has been traditionally assumed to be a class M alloy [17], an examination of Table I reveals that many of these observations are more characteristic of a class A response. These include measurements of $n \approx 3.0$–3.5 [11, 13, 16], recordings of inverse, linear and sigmoidal primary creep transients [5, 6, 11], and the existence of randomly oriented dislocations and ill-formed subboundaries in the deformed specimens [5, 13, 16].

Interestingly, Hedworth and Pollard [13] observed $n \approx 3$ at $T \approx 0.69 T_m$, whereas Evans and Wilshire [5] and Feltham and Copley [11] obtained $n \approx 4.5$ at the same temperature. Significantly, Table I reveals that values of $n < 4$ were observed only in the fine-grained alloys ($d \leq 50$ μm). It is worth noting that Svensson and Dunlop [18] reported a value of $n \approx 2.7$ for a fine-grained ($d \approx 15$ μm) Cu–21% Zn alloy for values of $\sigma/G < 10^{-3}$, where G is the shear modulus. Thus, if the effect of diffusion creep is negligible, then it is likely that these values of $n \approx 3.0$–3.5 are due to a viscous glide mechanism.

Because most of the experimental values of activation energy for creep, Q_c, (~ 160–175 kJ mol^{-1}, Table I) are similar to those predicted for dislocation climb and viscous glide mechanisms, which are identical to Cu–30% Zn and equal to about 180 kJ mol^{-1} (Equations A7 and A8), it is impossible to identify the rate-controlling processes solely on the basis of Q_c. In addition, other relevant information (e.g. the activation volume, V^*, the instantaneous strain, $\Delta\varepsilon$, after a stress change, and internal stress, σ_i) often used for identifying creep mechanisms are limited or nonexistent for this alloy. In particular, it is now known that $\Delta\varepsilon$ and σ_i are significantly different for class A and class M response (3, 19–21) so that the measurement of these parameters should be useful in distinguishing between the two types of creep behaviour.

The present study was undertaken to obtain detailed information on the creep behaviour of Cu–30% Zn at temperatures between 573 and 823 K (0.48–

0022–2461/91 $03.00 + .12

TABLE I A compilation of the creep properties of nominal Cu–30% Zn

Grain size (μm)	Homologous temperature[a]	Normalized stress[b] ($\times 10^{-4}$)	n	Activation energy (kJ mol^{-1})	Primary curve	Remarks	Reference
30	0.57 0.61 0.65 0.69	10.0–29.7 6.5–22.9 4.2–16.2 3.8–11.0	4.8 3.4 3.8 4.5	160	Their Fig. 3 suggests inverse or linear creep at $T \approx 0.61T_m$ for $\sigma/G < 1.5 \times 10^{-3}$. Norml transients under other conditions.	Values of n were obtained by replotting the original data double logarithmically.	[11]
190	0.68 0.71 0.75	5.7–6.9 5.8–8.3 5.9–8.5	5.0	129	Normal primary creep under all conditions.		[12]
5000	0.50 0.57 0.65 0.69	14.6–60.8 6.9–29.4 3.2–18.6 3.6–14.6	4.5	160–175	Sigmoidal at $T = 0.50$–$0.57T_m$ for $\sigma/G < 2 \times 10^{-3}$. Normal transients under other conditions.	Mostly random dislocations in the secondary creep region.	[5]
50	0.56 0.66 0.69	–	4.5 3.5 3.2	–	–	Values of n obtained from their Fig. 2. Paired dislocations, tangles and random dislocations observed in the secondary creep region.	[13]
5000–6000	0.53	12.7–26.8	–	–	Sigmoidal and inverse for $\sigma/G < 2 \times 10^{-3}$.		[6]
470	0.60	4.7–25.0	4.8	160	–	Dislocation pileups in the secondary creep region.	[14]
170	0.57	5.7–27.2	4.5	–	–		[15]
30	0.62	4.0	3.1	–	–	Random dislocations	[16]

[a] Test temperatures were normalized by the solidus temperature of 1188 K.
[b] The stresses were normalized by the shear modulus estimated from Equation A1

$0.70T_m$) in order to examine the possibility of a class M to class A to class M (or exponential creep) transition in this alloy.

2. Experimental procedure

Tensile specimens having gauge dimensions of 25.4 mm × 9.5 mm were machined from 2 mm thick hot-rolled sheets of composition 0.001 (wt %) Al, 0.005% Ag, 69.4% Cu, 0.015% Ni, 0.0023% O, 0.005% Pb, 0.01% Sn and 30.5% Zn. Prior to testing, the machined specimens were annealed either at 923 ± 1 K for 6 h or at 1023 ± 1 K for 5 h under a continuously flowing argon atmosphere to produce linear intercept grain sizes of 120 ± 10 μm or 335 ± 20 μm, respectively.

Constant stress creep tests were conducted from 573–823 K (0.48–$0.70T_m$) under a flowing argon atmosphere with both the temperature control and the temperature gradient maintained within ± 1 K. The strain was measured by a linear variable differential transducer and recorded on a strip chart recorder to an accuracy of about 10^{-4} and a resolution of about 5×10^{-5}. Other details of the testing procedure are given elsewhere [22].

Both stress change experiments and single tests on individual specimens were used for determining the stress dependence of the secondary creep rate, $\dot{\varepsilon}$. The creep rates measured by both techniques agreed to within a factor of 1.5. The apparent activation volume for creep was determined by measuring the creep rates before and after small stress changes ($\sim 0.05\sigma$) at various testing temperatures as described elsewhere [23]. These measurements were conducted both in the primary and in the secondary creep regimes, and V^* was calculated from the relationship

$$V^* = 2kT(\partial \ln \dot{\varepsilon}/\partial\sigma)_T \approx 2kT(\Delta \ln \dot{\varepsilon}/\Delta\sigma)_T \quad (1)$$

where k is Boltzmann's constant. The error in the determination of V^* was estimated to be about $\pm$ 10–20%.

Internal stress measurements were conducted using a stress reduction technique similar to that described by Pahutová *et al.* [24]. In these experiments, the

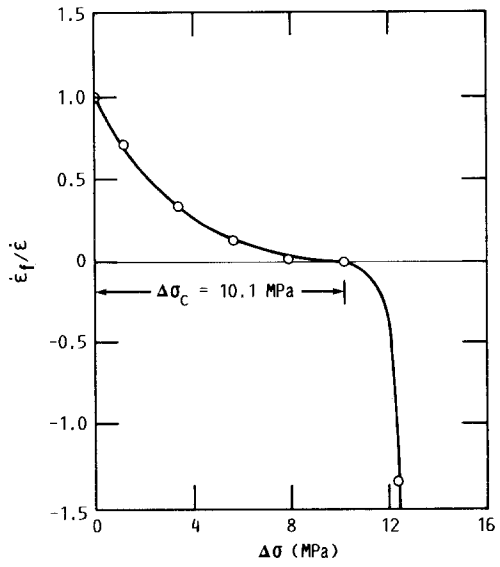

Figure 1 Plot of $\dot{\varepsilon}_f/\dot{\varepsilon}$ against $\Delta\sigma$ used for determining the internal stress at 823 K under an initial stress of 18.8 MPa. $d = 120\ \mu m$, $T = 823$ K, $\sigma = 18.8$ MPa, $\dot{\varepsilon} = 1.9 \times 10^{-5} s^{-1}$.

stress was decreased in a series of nominally equal steps (the period between the consecutive stress change was about 10 s), and the creep rate, $\dot{\varepsilon}_f$, immediately following each stress reduction was measured. The internal stress could then be determined from a plot of $\dot{\varepsilon}_f/\dot{\varepsilon}$ against $\Delta\sigma$, where in this case $\dot{\varepsilon}$ is the steady-state creep rate before the first stress reduction and $\Delta\sigma$ is the magnitude of the total stress change to that point. Thus

$$\sigma_i = \sigma - \Delta\sigma_c \quad (2)$$

where $\Delta\sigma_c$ is the value of $\Delta\sigma$ when $\dot{\varepsilon}_f/\dot{\varepsilon} = 0$ (Fig. 1).

Stress change experiments were also used to determine $\Delta\varepsilon$ and to characterize the nature of the creep transients following a stress change. As described elsewhere [25], these tests were conducted in the steady-state region by first reducing the stress in steps by almost equal amounts from σ_1 to σ_2, where σ_1 and σ_2 are the initial and the final magnitudes of the applied stress, and then reloading in the reverse order from σ_2 to σ_1.

3. Results

3.1. The shape of the creep curves

Depending on stress and temperature, either inverse, normal or sigmoidal primary creep curves were observed in all the tests except a few where linear creep was recorded (Fig. 2a and b). As shown in Fig. 2, the primary creep region is followed by a steady-state regime which is better defined in Cu–30% Zn than copper [22], where the total amount of steady-state creep strain decreases with decreasing stress (Fig. 2a) and temperature (Fig. 2b). In addition, the strain to reach steady-state increases with increasing stress and temperature.

The inverse and sigmoidal primary creep transients were observed at and above 623 K, and at stresses resulting in minimum creep rates between 10^{-7} and $2 \times 10^{-4} s^{-1}$; normal primary creep was observed

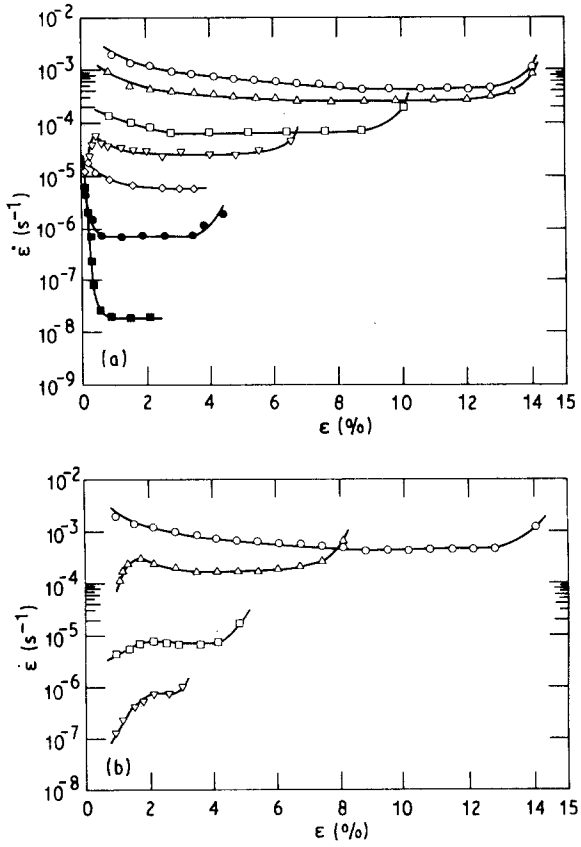

Figure 2 Variation of the creep rate with creep strain as a function of (a) stress and (b) temperature. (a) $d = 120\ \mu m$, $T = 823$ K, σ (MPa): ■ 4.5, (●) 10.0, (◇) 16.3, (▽) 23.2, (□) 28.1, (△) 42.6, (○) 51.0. (b) $d = 120\ \mu m$, $\sigma = 51.0$ MPa, T (K): (▽) 623, (□) 673, (△) 773, (○) 823.

under all other conditions. Although inverse primary creep curves were common at 623 K, and in one or two instances at 673 K when the stresses were high, they were not observed at higher temperatures. However, this type of primary creep behaviour lasted between 6 and 15 h in contrast to sigmoidal primary creep, which typically lasted between a few minutes and 4 h. Clearly, these results cannot be attributed to other effects such as a slack in the load train. Significantly, sigmoidal creep occurred only in annealed specimens but not in prestrained samples, which exhibited only normal primary creep transients even after relatively low amounts of prestrain of about 1.5% [26].

3.2. Stress dependence of the minimum creep rate

Because the strain in the secondary creep region was often quite small, it was necessary to assume that the minimum creep rate was representative of steady-state behaviour. Fig. 3 shows the variation of the minimum creep rate plotted against the applied stress double logarithmically, where the conditions under which inverse and sigmoidal primary creep behaviour occur are demarcated by the two broken curves. The stress exponent decreases from $n = 5.2 \pm 0.2$ below 623 K to $n = 4.1 \pm 0.2$ above 623 K (Fig. 3). As shown in Fig. 3, the steady-state creep rates are not significantly dependent on grain size in agreement with the earlier observations of Barrett *et al.* [27] on copper.

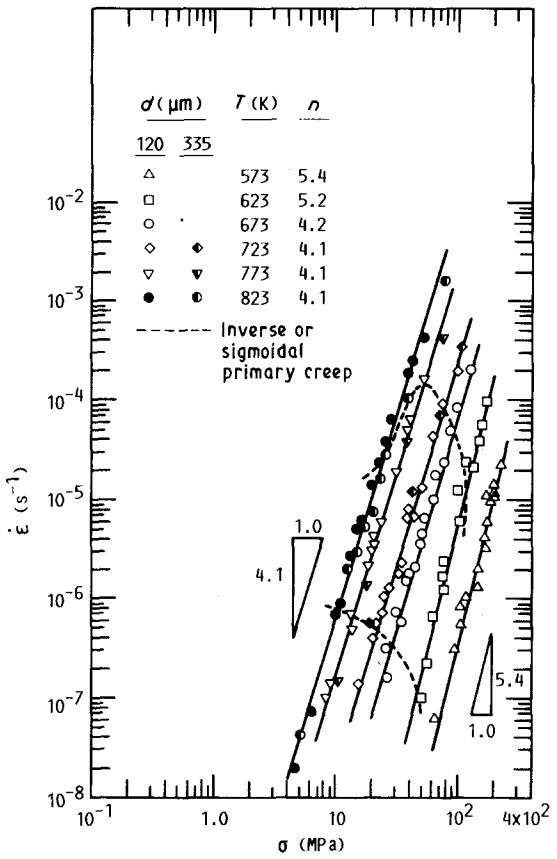

Figure 3 Double logarithmic plot of the minimum creep rate against the applied stress between 573 and 823 K. The broken curves enclose the region of the $\dot{\varepsilon}$–σ space where inverse or sigmoidal primary creep transients were observed.

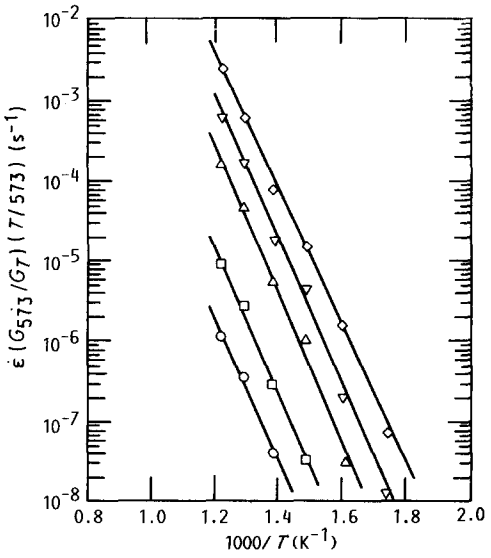

Figure 4 Variation of the temperature-compensated minimum creep rate against the inverse of the absolute temperature for values of normalized stress between 3×10^{-4} and 2×10^{-3}. σ/G and Q (kJ mol^{-1}), respectively: (○) 3.0×10^{-4}, 180 ± 15; (□) 5.0×10^{-4}, 180 ± 15; (△) 1.0×10^{-3}, 175 ± 20; (▽) 1.4×10^{-3}, 170 ± 20; (◇) 2.0×10^{-3}, 170 ± 20.

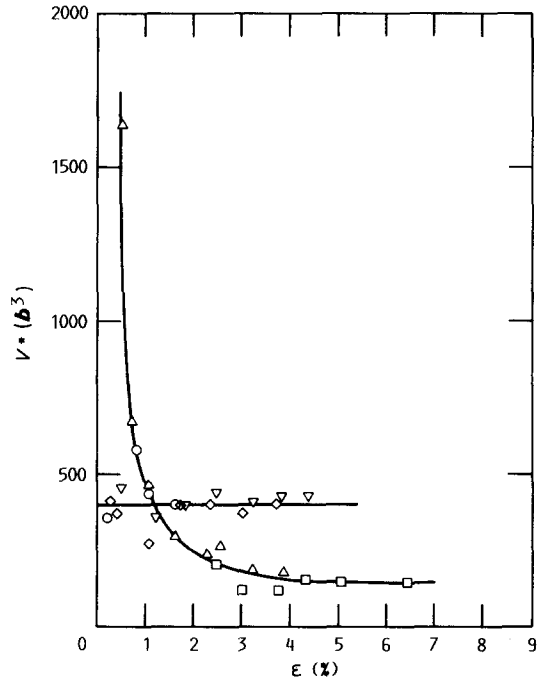

Figure 5 Strain dependence of the apparent activation volume for creep showing two types of creep behaviour. $d = 120$ μm, T (K) and σ (MPa), respectively: (□) 623, 61.5; (△) 708, 37.8; (▽) 773, 24.6; (◇) 773, 23.5; (○) 823, 15.6.

3.3. Activation energy for creep

The true activation energy for creep was determined from Fig. 3 by cross-plotting the temperature-compensated creep rate against the inverse of the absolute temperature for different values of normalized stress (Fig. 4). The values of Q_c are tabulated in Fig. 4, where it is seen that they range from $Q_c \approx 180 \pm 15$ kJ mol^{-1} at $\sigma/G \approx 3.0 \times 10^{-4}$ to $Q_c \approx 170 \pm 20$ kJ mol^{-1} at $\sigma/G \approx 2.0 \times 10^{-3}$ (Fig. 4). The magnitudes of Q_c are in reasonable agreement with almost all the results shown in Table I within experimental error. They also agree very well with the identical activation energies of about 180 kJ mol^{-1} estimated for dislocation climb and viscous glide creep mechanisms in this alloy (Equations A7 and A8 in the Appendix).

3.4. Activation volume for creep

Fig. 5 shows the variation of V^* with strain, where V^* is expressed in terms of the Burgers vector, $b \approx 2.56 \times 10^{-10}$ m. Two modes of behaviour are apparent. At the lower temperatures and higher stresses, V^* decreases strongly with increasing strain from values of $V^* \approx 1700 b^3$ at $\varepsilon \approx 0.5\%$ to $V^* \approx 100 b^3$ for $\varepsilon > 3\%$ probably due to a corresponding increase in the obstacle density. However, a constant and strain independent value of $V^* \approx 400\ b^3$ is observed when $T \geq 773$ K and $\sigma \leq 24.6$ MPa. It should be noted that V^* is expected to be independent of strain for both dislocation climb and viscous glide-controlled mechanisms. These two modes of strain dependencies were also reported for copper, although in this case $V^* \approx 1600$–$1700 b^3$ at the higher temperatures and lower stresses corresponding to the strain independent region [22, 23]. A non-linear stress dependence of V^* is observed in the secondary creep region, where the data are independent of temperature (Fig. 6).

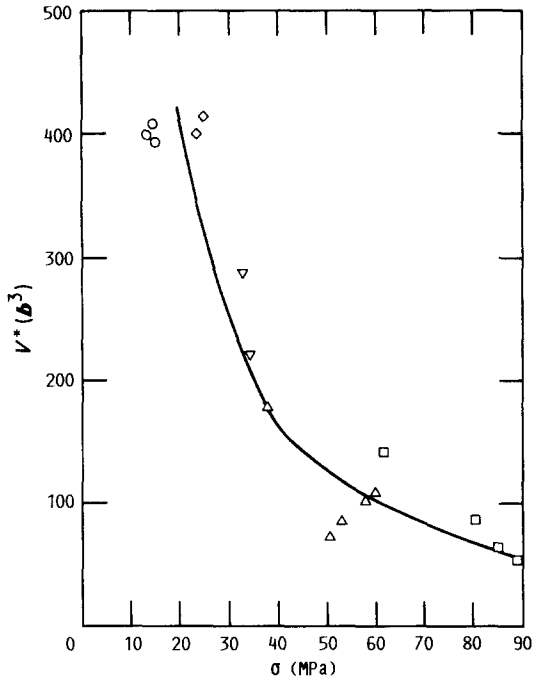

Figure 6 Stress dependence of the apparent activation volume in the secondary creep region. $d = 120\ \mu m$, T (K): (□) 626, (△) 707, (▽) 748, (◇) 773, (○) 823.

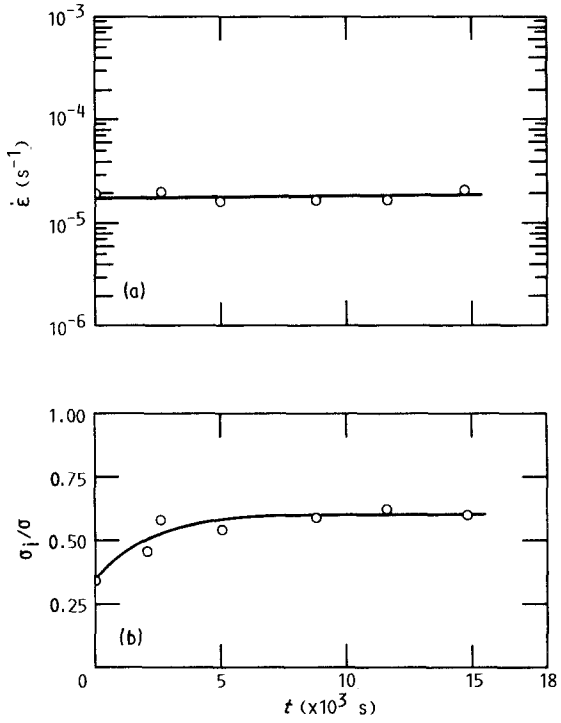

Figure 7 Variation of (a) the creep rate and (b) the normalized internal stress with time. $d = 120\ \mu m$, $T = 823$ K, $\sigma = 18.8$ MPa.

3.5. Internal stress and instantaneous strain

Fig. 7a and b show the variation of $\dot{\varepsilon}$ and σ_i/σ with time, t, respectively, at 823 K under a stress of 18.8 MPa. Although these conditions generally resulted in sigmoidal primary creep, a linear creep curve with an essentially constant creep rate was observed in this particular experiment (Fig. 7a). Despite a constant creep rate, the internal stress rises from an initial value of about $0.35\,\sigma$ to a constant value of about $0.6\,\sigma$ during the first hour of the test (Fig. 7b). It is worth noting that observations on Cu–16 (at %) Al during sigmoidal creep also resulted in an increase in σ_i/σ with time from $\sigma_i/\sigma \approx 0.3$ in the inverse portion of the primary curve to $\sigma_i/\sigma \approx 0.9$ in the normal part of the primary transient [7].

The magnitude of σ_i/σ decreases with increasing applied stress in the secondary creep region from $\sigma_i/\sigma \approx 0.6$ at $\sigma = 18.8$ MPa in the sigmoidal creep region to $\sigma_i/\sigma \approx 0.4$ at $\sigma = 32.9$ MPa in the normal creep regime (Fig. 8). Similar trends are observed for other alloys: Al–5.5 (at %) Mg [28], Cu–30% Zn [14], Fe–1.8 (at %) Mo [8] and Fe–4.1 (at %) Mo [29]. It should be noted that a value of $n \approx 3$ was observed for Al–5.5% Mg and Fe–4.1% Mo for the conditions shown in Fig. 8. In addition, although Oikawa *et al.* [8] originally reported a value of $n \approx 4$ for the Fe–1.8% Mo alloy, a recent study showed that $n \approx 3.4$ when $6 \leq \sigma \leq 30$ MPa for an alloy of similar composition while class M behaviour was observed when $\sigma < 6$ MPa and $\sigma > 30$ MPa [10]. Because values of $\sigma_i/\sigma \approx 1$, which correlate very well with the formation of cell or subboundaries [7], are characteristic of class M behaviour [3], it would appear from Fig. 8 that Cu–30% Zn does not exhibit class M behaviour above $\sigma \approx 10$ MPa (i.e. $\sigma/G \approx 3 \times 10^{-4}$).

The variation of $\Delta\varepsilon$ with $\Delta\sigma/\sigma$ is non-linear in the sigmoidal creep region (Fig. 9). It should be noted that because $\Delta\varepsilon$ is much larger than the elastic strain calculated from the relation $\Delta\varepsilon = \Delta\sigma/E$, where the Young's modulus, $E \approx 8.4 \times 10^4$ MPa at 823 K [12], the instantaneous strain has a significant plastic strain component. These results are similar to those reported for Al, Al–5 (at %) Mg and Al–5 (at %) Zn [21]. More importantly, observations on other solid solution alloys reveal that $\Delta\varepsilon^+ \approx \Delta\varepsilon^-$, where $\Delta\varepsilon^+$ and $\Delta\varepsilon^-$ are the magnitudes of $\Delta\varepsilon$ after a stress increase and a stress decrease, respectively, whenever viscous glide controls creep behaviour [19–21]. In contrast, creep controlled by dislocation climb results in $\Delta\varepsilon^+ \gg \Delta\varepsilon^-$.

4. Discussion

4.1. Comparison of the creep data with other investigations

The magnitudes of $n \approx 4.1$–5.4 obtained in this investigation are consistent with the values of $n > 4$ shown in Table I. Additionally, with the exception of the data reported by Bonesteel and Sherby [12], the activation energies for creep of this alloy, which vary between 170 and 180 kJ mol^{-1} (Fig. 5), are in reasonable agreement with those tabulated in Table I, as well as with those given by Equations A7 and A8.

As illustrated in Fig. 10 and noted in Section 1, the magnitudes of the stress exponents reported for Cu–30% Zn (Table I) approach $n \approx 3$ when $d < 50\ \mu m$. In order to test whether diffusion creep may have influenced some of these results, creep data obtained at 723 and 823 K in this and other investigations [11, 14] were compared with the predicted creep rates for Coble creep [30] when $d = 30\ \mu m$ (Fig. 11). The theoretical creep rates were calculated using the equation modified by Langdon and Mohamed [31]. Similar calculations showed that the predicted creep rates for Nabarro–Herring creep [32, 33] were less

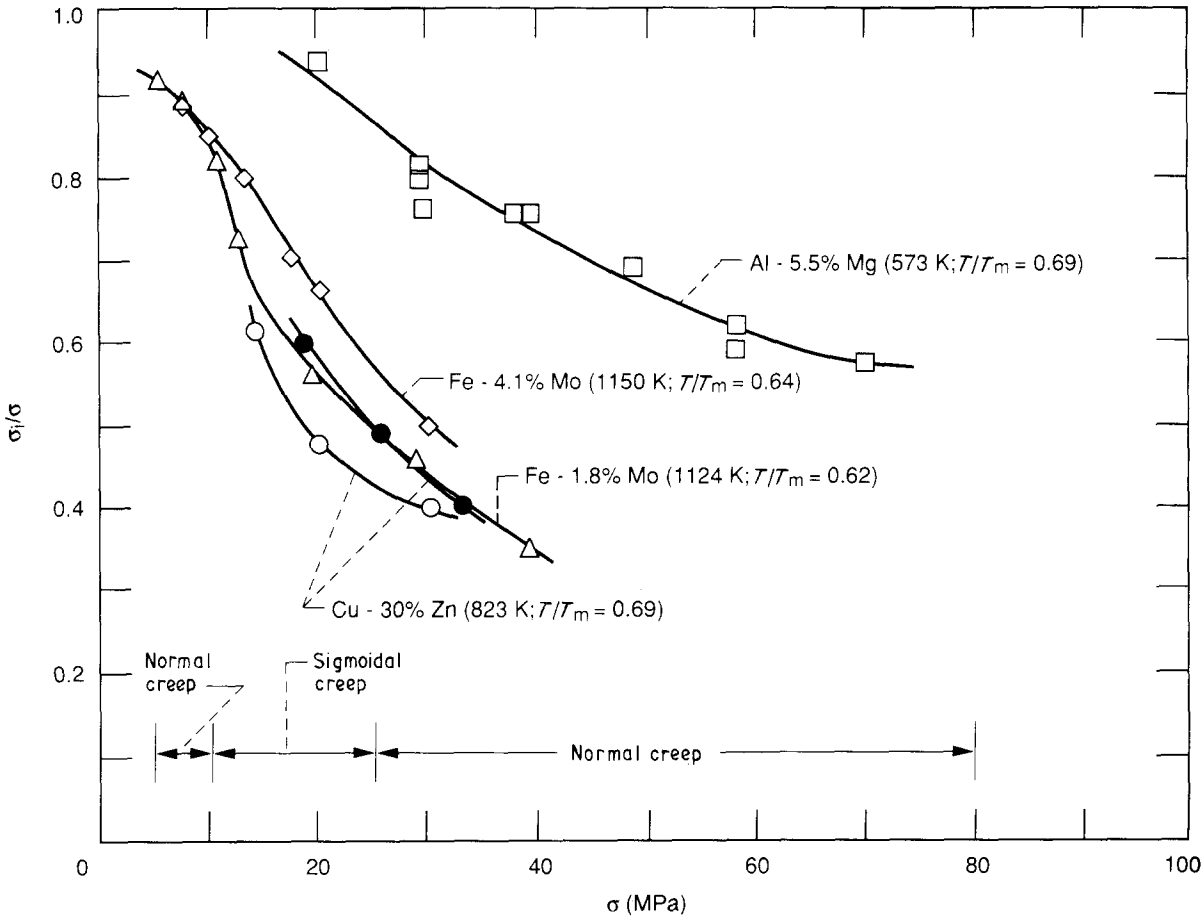

Figure 8 Plot of σ_i/σ against σ under steady-state creep for several solid solution alloys: Al–5.5 (at %) Mg [28], Cu–30% Zn ([14], present work), Fe–1.8 (at %) Mo [8] and Fe–4.1 (at %) Mo [29]. The range of stresses where normal or sigmoidal primary creep occurred in this study at 823 K is demarcated in the figure. (○) [14], (△) [8], (□) [28], (◇) [29], (●) present work.

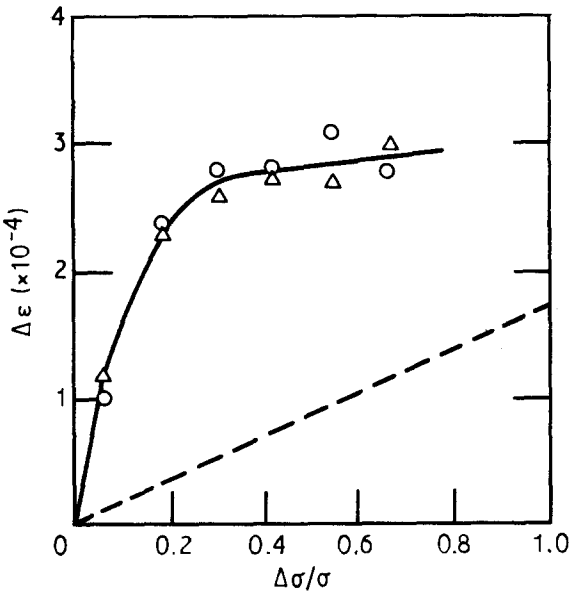

Figure 9 Plot of $\Delta\varepsilon$ against $\Delta\sigma/\sigma$ showing that $\Delta\varepsilon^+ \approx \Delta\varepsilon^-$. $d = 120\,\mu m$, $T = 823$ K, $\sigma = 18.8$ MPa. (○) Stress decrease, (△) stress increase, (– – –) elastic strain.

than $10^{-8}\,s^{-1}$. It is clear from Fig. 11 that the data from the three investigations are in reasonable agreement with each other so that the creep rate is essentially independent of grain size. Furthermore, the experimental data lie well below the lines for Coble creep and show no deviation towards a slope of $n = 1$. Therefore, it is concluded that the values of $n \approx 3$ shown in Table I were not influenced by diffusion creep and appear to be due to a viscous glide-controlled process. (The influence of grain-boundary sliding is discounted because the stress exponent for sliding was found to be similar to that for creep [34].) In the absence of a well-defined viscous glide region, it is useful to examine whether the upper and lower boundaries demarcating the sigmoidal/inverse creep region (Fig. 3) coincide with the expected class M to class A to class M transition stresses.

4.2. Evaluation of the transition stresses

If it is assumed that Cu–30% Zn exhibits transitions from class M to class A to class M (or exponential creep) behaviour with increasing stress, then the normalized transition stresses can be calculated easily. A transition from a climb to a viscous glide-controlled creep occurs when

$$\dot{\varepsilon}_c = \dot{\varepsilon}_g \tag{3}$$

where $\dot{\varepsilon}_c$ and $\dot{\varepsilon}_g$ are the creep rates for the dislocation climb and viscous glide mechanisms, respectively. The creep rate for a dislocation climb-controlled process is given by

$$\dot{\varepsilon}_c = A_c(\tilde{D}_c G\boldsymbol{b}/kT)(\sigma/G)^n \tag{4}$$

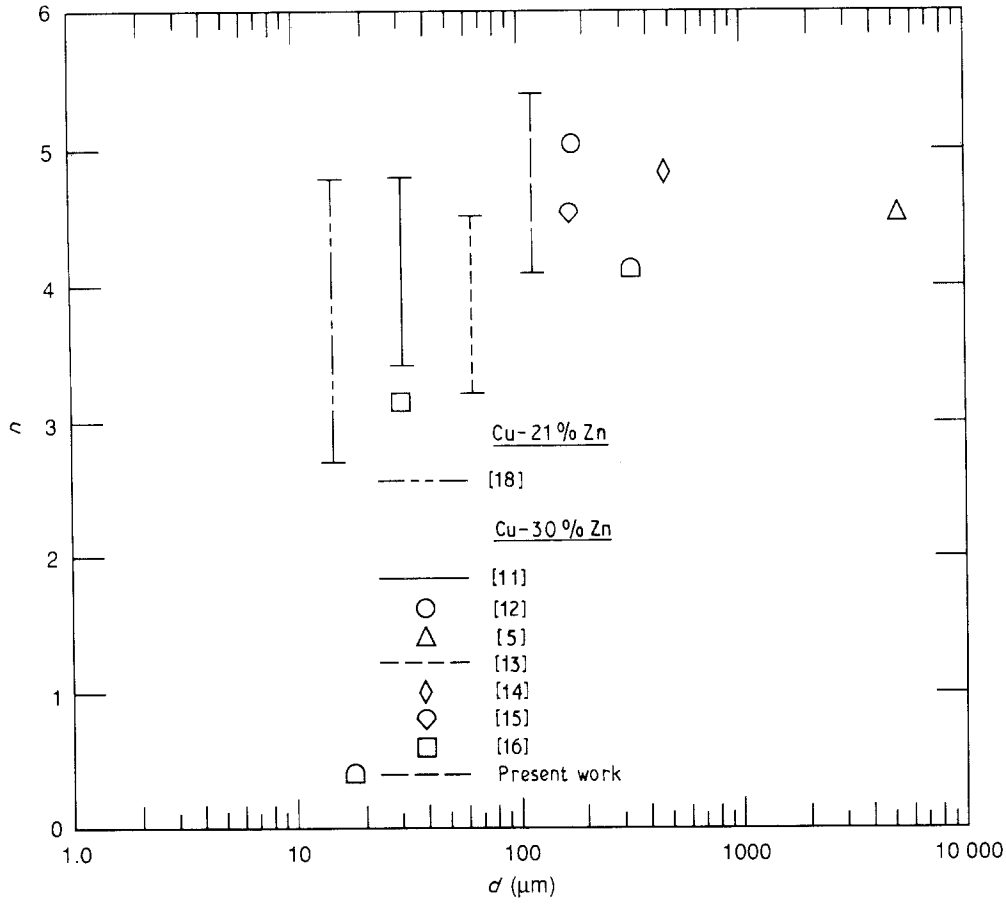

Figure 10 Plot of compiled values of n against d for Cu–21% Zn and Cu–30% Zn showing $n \approx 3$ are observed only when $d < 50$ μm. The present data are compared with those from other investigations.

where $\tilde{D}_c$ is the complex diffusion coefficient for climb and A_c is a dimensionless constant estimated to be about 140 for Cu–30% Zn when $n \approx 4.1$ (Fig. 3).

Several viscous glide-controlled mechanisms exist depending on the nature of the dislocation–solute interaction and each of them contribute to the total creep rate [35]. Thus,

$$\dot{\varepsilon}_g = \Sigma_i A_{gi}(\tilde{D}_g G\boldsymbol{b}/kT)(\sigma/G)^3 \quad (5)$$

where $\tilde{D}_g$ is the complex diffusion coefficient for viscous glide and A_{gi} is a dimensionless constant for the ith process. Because these mechanisms act sequentially, the slowest process will be rate-controlling (i.e. the one with the smallest value of A_{gi} [35]). The equations and the magnitudes of A_{gi} for each viscous glide process are listed in Table II, where the parameters used in making these estimates for Cu–30% Zn are tabulated in Table III along with the corresponding reference sources. It is clear that A_{gi} is the lowest for the Cottrell–Jaswon (C–J) solute drag mechanism for which $A_{C-J} \approx 0.07$ (Table II). Although Evans and Wilshire [5, 6] suggested that sigmoidal and inverse primary transients occur in Cu–30% Zn due to short-range ordering, it is clear from Table II that because $A_F \gg A_{C-J}$, this mechanism is unimportant in this alloy. Thus, with $\tilde{D}_g \approx \tilde{D}_c$ (Equations A7 and A8), $n = 4$, $A_c \approx 140$ and $A_{C-J} \approx 0.07$, the transition normalized stress, $(\sigma/G)_{tr}$, estimated from Equations 3–5 is about 5×10^{-4}. This corresponds to predicted transition stresses of about 17 and 19 MPa at 823 and 623 K, respectively. Noting that any tendency towards class A behaviour should correspond to the region between the broken curves in Fig. 3, these calculated values of transition stress lie either well inside this regime (e.g. 823 K) or much below the lower boundary (e.g. 623 K). If the latter boundary is assumed to represent the class M to class A transition point, then the transition stress, σ_{tr}, as estimated from Fig. 3, is likely to be about 10 and 45 MPa at 823 and 623 K, respectively. Thus, the discrepancy between these and the calculated values of σ_{tr} is within a factor of 2.5.

The class A to class M (or exponential creep) transition occurs when the dislocation breaks away from its solute atmosphere at a breakaway stress, σ_b, given by [44]

$$\sigma_b = [(W_m)^2 X_B]/(5\boldsymbol{b}^3 kT) \quad (12)$$

where X_B is the mole fraction of the solute, and W_m is the binding energy between the solute atom and the dislocation given by [44]

$$W_m = (1/2\pi)[(1 + \nu)/(1 - \nu)]G|\delta V_a| \quad (13)$$

where ν is the Poisson's ratio and $|\delta V_a|$ is the difference in volume between the solute and the solvent atoms. The estimated value of $|\delta V_a| \approx 9 \times 10^{-31}\,m^3$ assuming that the atomic radii of copper and zinc atoms are 1.35×10^{-10} m and 1.31×10^{-10}, respectively [45]. Thus, $\sigma_b \approx 24.9$ and 41.1 MPa at 823 and 623 K, respectively, for $X_B = 0.29$, $k = 1.38 \times 10^{-23}\,J\,K^{-1}$ and $\nu \approx 0.3$. Assuming that the experimental transition stresses can be estimated from the upper boundary of the sigmoidal/inverse creep region in

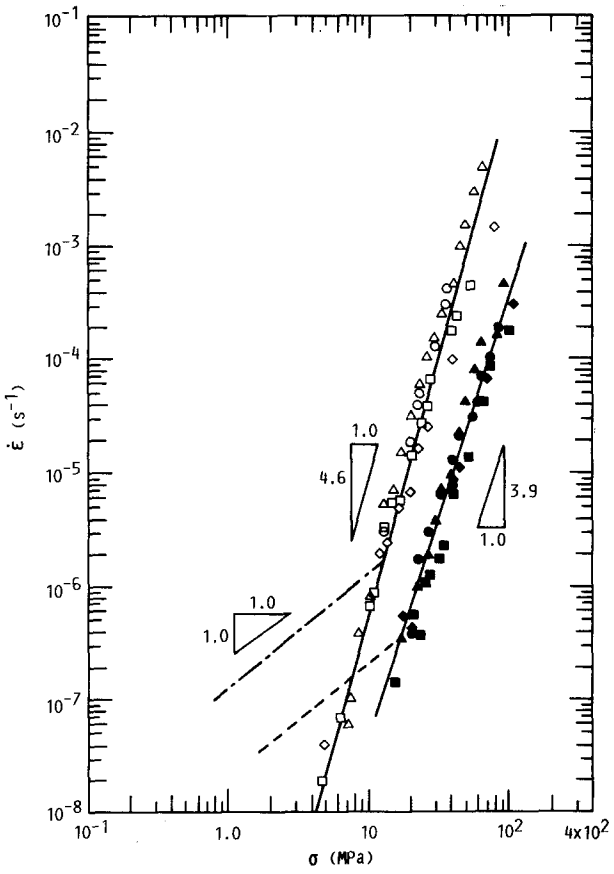

Figure 11 Comparison of (■, □, ◆, ◇) present results, d = (■, □) 120 μm, (◆, ◇) 335 μm, with the creep data reported by (●, ○) Feltham and Copley [11] d = 30 μm, and (▲, △) Hostinský and Čadek [14] d = 470 μm for Cu–30% Zn at 723 K (solid symbols) and 823 K (open symbols). (– – –, ——————). Calculated values of the creep rate for Coble creep.

Fig. 3, these values of σ_b are about 24 and 100 MPa at 823 and 623 K, respectively; thus, while the calculated and the experimental results are in excellent agreement at 823 K, there is a large discrepancy between the two values at 623 K.

Thus, the calculated magnitudes of σ_{tr} and σ_b do not agree very well with those estimated from the lower and upper boundaries shown in Fig. 3. This disagreement is consistent with the absence of a well-defined class M to class A to class M transition (Fig. 3).

4.3. Concluding remarks

As a result, it can be argued that the values of $n \approx 4.1$ (Fig. 3) and the strain independence of V^* (Fig. 5) are consistent with the idea that dislocation climb dominates steady-state creep at the higher temperatures and lower stresses. Thus, the sigmoidal primary creep curves should signify a transition in the rate-controlling mechanism from viscous glide in the initial stages of creep to dislocation climb in the steady-state [46], while the equality, $\Delta\varepsilon^+ \approx \Delta\varepsilon^-$ (Fig. 9), should indicate the importance of viscous glide during transient creep [3].

However, many of the observations reported in this paper or documented in the literature (Table I) are inconsistent with the characteristics of ideal class M behaviour [2]. First, the occurrence of inverse creep in this (Fig. 2b) and another study [6] denotes that steady-state creep is controlled by viscous glide under some conditions [46]. Second, the fact that $\sigma_i/\sigma \ll 1$ in the sigmoidal creep region at 823 K is consistent with a class A rather than class M response (Figs 7b and 8). Third, it was demonstrated in Section 4.1 that the values of $n \approx 3.0$–3.5 [11, 13, 16] given in Table I cannot be attributed to the added contribution from diffusion creep mechanisms to dislocation climb. Fourth, large instantaneous strains ($\Delta\varepsilon \approx 5 \times 10^{-3}$) were observed at 823 K in Cu–30% Zn whenever the stress was changed across the upper sigmoidal–normal creep boundary (Fig. 3), but not within the sigmoidal creep region, where almost identical stress changes yielded values of $\Delta\varepsilon \approx 3 \times 10^{-4}$ [25]. In addition, while inverse strain transients were observed after a stress increase in the sigmoidal regime, they changed to normal creep when the stress was increased across the upper boundary. These results suggest that the dislocations had broken away from or were captured by their solute atmospheres when the stress was increased or decreased across this boundary, respectively [25].

The picture that emerges from this discussion is that Cu–30% Zn does not exhibit either an ideal class A or class M behaviour, and therefore the existing classification schemes are inadequate in characterizing this alloy. The reasons for this deviation from ideal behaviour are not entirely clear but they may be due to the high solute content in the alloy. Because Cu–16 (at %)

TABLE II The estimated magnitudes of A_{gi} in Equation 5 for different viscous glide mechanisms[a]

Mechanism	Equation		A_{gi}
1. Cottrell–Jaswon locking	$A_{C-J} = (0.35/e^2 X_B)(kT/Gb^3)^2$	(6)	0.07
2. Fisher short-range order	$A_F = (0.05kT)/(X_A X_B \alpha_s E_b)$	(7)	10.0
	where		
	$E_b = (kT/2)\ln\{(X_A + X_B\alpha_s)(X_B + X_A\alpha_s)/[X_A X_B(1-\alpha_s)^2]\}$	(8)	
3. Suzuki locking	$A_s = 0.4 - (kTE_s)/[(\Gamma_A - \Gamma_B)^2 V_m b]$	(9)	20.0
	where		
	$E_s = (\delta S/\delta S_{id})\{(RT/X_A X_B) + [(8G/9V_m)(dV_m/dX_B)^2 - 8\delta H_{1/2}]\}$	(10)	
4. Snoek stress-induced ordering	$A_{sn} = (125/\delta_i)(kT/Gb^3)$	(11)	50.0

[a] The mechanisms and equations are discussed in detail by Mohamed [35]. The definitions of the parameters and their magnitudes are given in Table III.

TABLE III The definitions and magnitudes of the parameters used for estimating A_{gi} in Table II

Symbol	Definition	Magnitude	Remarks	Reference
a	Lattice parameter	3.68×10^{-10} m		[36]
E_b	Bond energy	1.1–1.6 kJ mol^{-1}	These values were estimated from Equation 8 in Table II for 573–823 K	
E_s	Chemical interaction energy	78 kJ mol^{-1}	Estimated from Equation 10 in Table II	
e	Atom misfit ratio	0.054		[37]
$\delta H_{1/2}$	Enthalpy of mixing of Cu–50% Zn	9.71 kJ mol^{-1}		[38]
N	Avogadro's number	6.022×10^{23} mol^{-1}		[39]
δS	Excess entropy of formation of a solid solution alloy	-2.12 kJ mol^{-1} K^{-1}		[38]
δS_{id}	Entropy of formation of an ideal solution	2.95 kJ mol^{-1} K^{-1}		[38]
V_m	Molar volume	7.5×10^{-6} m^3 mol^{-1}	$V_m = Na^3/4$ for fcc metals and alloys	[36]
$\frac{dV_m}{dX_B}$	Rate of change in the molar volume with solute concentration	7.6×10^{-12} m^3 mol^{-2}	Estimated from a–X_B plot	[36]
X_B	Mole fraction of solute	0.29		
α_s	Degree of short range order	0.1	This value of α_s represents an upper bound	[40]
Γ_A	Stacking fault energy of solvent	0.055 J m^{-2}		[41]
Γ_B	Stacking fault energy of solute	0.14 J m^{-2}		[42]
δ_i	Strength of the internal friction peak	0.03 at 573 K		[43]

Al [7] and Cu–30% Zn show similar creep characteristics, it is likely that other solid solution alloys containing large amounts of solute will also exhibit non-ideal behaviour. Therefore, it may be more appropriate to classify them as class I (intermediate type) alloys.

Finally, double logarithmic plots of $\dot{\varepsilon}kT/\tilde{D}_g Gb$ against σ/G revealed that the data with $n > 5$ (Fig. 3) lie in the exponential creep region. A similar observation was reported for copper [22]. The decrease in V^* with increasing strain (Fig. 5) therefore appears to result from an increase in the obstacle density and a corresponding decrease in the activated distance.

5. Conclusions

1. Inverse, linear and sigmoidal primary creep curves were observed above 573 K at stresses corresponding to a range of minimum creep rates between 10^{-7} and 2×10^{-4} s^{-1}. Normal primary creep transients were obtained under other stress and temperature conditions.

2. The stress exponent for creep of Cu–30% Zn decreases from about 5.4 at 573 K to about 4.1 above 673 K, while the true activation energy for creep is about $Q_c \approx 175$ kJ mol^{-1}.

3. The apparent activation volume for creep decreases with increasing strain at the lower temperatures and higher stresses, while it is relatively independent of strain at the higher temperatures and lower stresses. It decreases non-linearly with increasing stress in the secondary creep region.

4. The magnitude of the instantaneous strain following a stress increase equals that after a stress decrease. In addition, the internal stress is about 40%–60% of the applied stress.

It is concluded from the present investigation, as well as from other published results, that Cu–30% Zn does not show a well-defined class M to class A to class M transition with increasing stress. The alloy has creep properties which are characteristic of both class A and class M behaviour under nominally similar stress and temperature conditions. Therefore, it is proposed that it be classified as a class I (intermediate type) alloy.

Appendix

A1. Values of shear modulus

The shear modulus, G, for Cu–30% Zn was assumed to vary linearly with temperature. The Young's modulus, E, data reported by Bonesteel and Sherby [12] were converted to G using the isotropic relation $G = 2E(1 + \nu)$ where Poisson's ratio, ν, was assumed to be 0.3. A linear regression line through the converted data gave

$$G = 5.05 \times 10^4 - 20T \qquad \text{(A1)}$$

where G is in MPa.

A2. Evaluation of the diffusion equations

In order to identify the creep mechanism, it is often necessary to know the activation energy for self diffusion. For solid solution alloys, three sets of equations are used to distinguish between dislocation climb and viscous glide-controlled mechanisms. The simplest of

these are the intrinsic diffusion coefficients of the solute and solvent atoms in the alloy. The intrinsic diffusion coefficients of copper and zinc in Cu–30% Zn were estimated by re-plotting diffusion data taken from several sources [47–49] (Fig. A1). The tracer diffusion coefficients, D_i^* were converted to intrinsic diffusion coefficients, D_i, through the relation

$$D_i = D_i^*[1 + \mathrm{d}(\ln \gamma_i)/\mathrm{d}(\ln N_i)] \quad \text{(A2)}$$

where γ_i is the activity coefficient of the ith species and N_i is the atom fraction of the ith component. The quantity $\mathrm{d}(\ln \gamma_i)/\mathrm{d}(\ln N_i)$ was estimated from a plot of the experimental values of γ_i against N_{Zn} using the data reported by Fisher *et al.* [50]. The following expressions were obtained from the lines of best fit through the data shown in Fig. A1

$$D_{Cu} = 8.4 \times 10^{-5} \exp(-175/RT) \quad \text{(A3)}$$

$$D_{Zn} = 1.0 \times 10^{-4} \exp(-165/RT) \quad \text{(A4)}$$

where R is the universal gas constant equal to 0.0083 kJ mol^{-1}, and D_{Cu} and D_{Zn} are in m^2 s^{-1}. Although Equations A3 and A4 are simple to use, they are generally not suitable for analysing creep data partly because both diffusing species can contribute to the creep mechanism and partly because they do not consider dislocation–solute interactions. As a result, two complex diffusion coefficients, $\tilde{D}_{HW}$ and $\tilde{D}$, are commonly used for analysing creep data of binary solid solution alloys under climb-controlled and viscous glide-controlled conditions, respectively [51]. Using the equations described by Mohamed and Langdon [51], these diffusion coefficients for Cu–30% Zn are

$$\tilde{D}_{HW} = 6.0 \times 10^{-5} \exp(-170/RT) \quad \text{(A5)}$$

$$\tilde{D} = 1.0 \times 10^{-4} \exp(-165/RT) \quad \text{(A6)}$$

However, Equations A5 and A6 are inappropriate for analysing creep behaviour of solid solution alloys because they do not consider the localized interaction of a single dislocation with a solute atmosphere [52–54]. Thus, using the equations proposed by Fuentes-Samaniego *et al.* [52, 53], the complex diffusion coefficients, $\tilde{D}_c$ and $\tilde{D}_g$, for climb and glide, respectively, in Cu–30% Zn are given by

$$\tilde{D}_c = 1.5 \times 10^{-4} \exp(-180/RT) \quad \text{(A7)}$$

$$\tilde{D}_g = 1.5 \times 10^{-4} \exp(-180/RT) \quad \text{(A8)}$$

Although Equations A7 and A8 were used in this investigation for analysing the creep data, it is interesting to note that the activation energies predicted by Equations A3–A8 are in reasonable agreement with each other, as well with Q_c (Table I and Fig. 5) within experimental error.

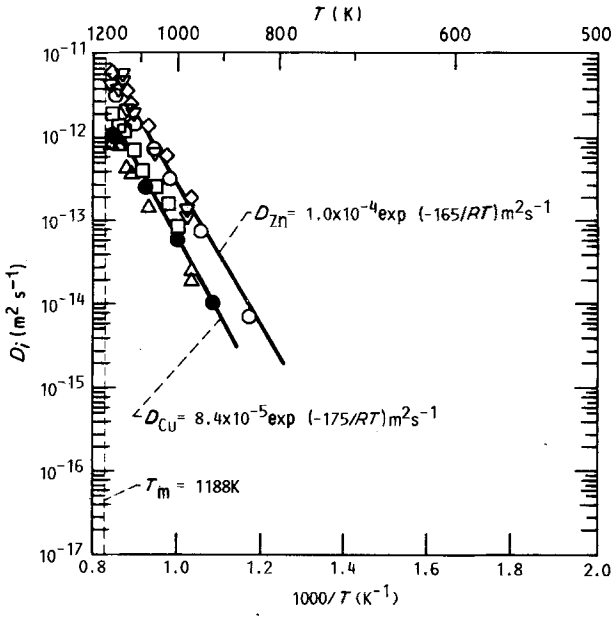

Figure A1 Intrinsic diffusion data for (△, ●, □) Cu and (▽, ○, ◇) Zn in Cu–30% Zn [47–49]. Method: (△, ▽) diffusion couple [47], (●, ○) tracer [48], (□, ◇) tracer [49].

Acknowledgements

The author thanks Professor T. G. Langdon, University of Southern California, for the use of his research facilities and for providing the material used in this investigation. He also thanks Professor A. K. Mukherjee, University of California, Davis, for permission to include the unpublished data in Table I, and Drs Mike Nathal and Dan Whittenberger for their helpful comments on the paper. Financial support for this study was provided in part by the United States Department of Energy and in part by the NASA Lewis Research Center under Co-Operative Agreement NCC 3-151.

References

1. P. YAVARI, F. A. MOHAMED and T. G. LANGDON, *Acta Metall.* **29** (1981) 1495.
2. T. G. LANGDON, in "Strength of Metals and Alloys (ICSMA 6)", edited by R. C. Gifkins (Pergamon Press, Oxford, 1983) p. 1105.
3. H. OIKAWA and T. G. LANGDON, in "Creep Behaviour of Crystalline Solids", Vol. 3, "Progress in Creep and Fracture", edited by B. Wilshire and R. W. Evans, (Pineridge Press, Swansea, 1985) p. 33.
4. H. OIKAWA, in "Creep and Fracture of Engineering Materials and Structures", edited by B. Wilshire and R. W. Evans (Pineridge Press, Swansea, 1987) p. 99.
5. W. J. EVANS and B. WILSHIRE, *Metall. Trans.* **1** (1970) 2133.
6. *Idem, Scripta Metall.* **8** (1974) 497.
7. T. HASEGAWA, Y. IKEUCHI and S. KARASHIMA, *Met. Sci. J.* **6** (1972) 78.
8. H. OIKAWA, D. MIZUKOSHI and S. KARASHIMA, *Metall. Trans.* **A9** (1978) 1281.
9. H. OIKAWA and S. NANBA, *Trans. Iron Steel Inst. Jpn* **27** (1987) 402.
10. S. NANBA and H. OIKAWA, *Mater. Sci. Engng* **101** (1988) 31.
11. P. FELTHAM and G. J. COPLEY, *Phil. Mag.* **5** (1960) 649.
12. R. M. BONESTEEL and O. D. SHERBY, *Acta Metall.* **14** (1966) 385.
13. J. HEDWORTH and G. POLLARD, *Metal Sci. J.* **5** (1971) 41.
14. T. HOSTINSKÝ and J. ČADEK, *Phil. Mag.* **31** (1975) 1177.
15. G. NELMES and B. WILSHIRE, *Scripta Metall.* **10** (1976) 697.
16. B. HIDALGO-PRADA and A. K. MUKHERJEE, unpublished research (1983).
17. O. D. SHERBY and P. M. BURKE, *Prog. Mater. Sci.* **13** (1967) 325.
18. L. E. SVENSSON and G. L. DUNLOP, *Metal Sci.* **16** (1982) 57.
19. H. OIKAWA, *Phil. Mag.* **37** (1978) 707.

20. H. OIKAWA and K. SUGAWARA, *Scripta Metall.* **12** (1978) 85.
21. T. G. LANGDON and P. YAVARI, in "Creep and Fracture of Engineering Materials and Structures", edited by B. Wilshire and D. R. J. Owen (Pineridge Press, Swansea, 1981) p. 71.
22. S. V. RAJ and T. G. LANGDON, *Acta Metall.* **37** (1989) 843.
23. S. V. RAJ, *J. Mater. Sci.* **24** (1989) 3196.
24. M. PAHUTOVÁ, J. ČADEK and P. RYŠ, *Scripta Metall.* **11** (1977) 1061.
25. S. V. RAJ, *ibid.* **20** (1986) 1751.
26. *Idem, J. Mater. Sci. Lett.* **7** (1988) 1342.
27. C. R. BARRETT, J. L. LYTTON and O. D. SHERBY, *Trans. AIME* **239** (1967) 170.
28. H. OIKAWA and A. YASUDA, *Metal Sci.* **13** (1979) 551.
29. H. OIKAWA, M. SAEKI and S. KARASHIMA, *Trans, Jpn Inst. Metals* **21** (1980) 301.
30. R. L. COBLE, *J. Appl. Phys.* **34** (1963) 1679.
31. T. G. LANGDON and F. A. MOHAMED, *Mater. Sci. Engng* **32** (1978) 103.
32. F. R. N. NABARRO, in "Report of a Conference on Strength of Solids" (The Physical Society, London, 1948) p. 75.
33. C. HERRING, *J. Appl. Phys.* **21** (1950) 437.
34. S. V. RAJ, *J. Mater. Sci.*, in press.
35. F. A. MOHAMED, *Mater. Sci. Engng* **61** (1983) 149.
36. T. B. MASSALSKI and J. E. KITTL, *J. Austral. Inst. Metals* **8** (1963) 91.
37. H. W. KING, *J. Mater. Sci.* **1** (1966) 79.
38. R. HULTGREN, R. L. ORR, P. D. ANDERSON and K. KELLEY, in "Selected Values of Thermodynamic Properties of Metals and Alloys" (Wiley, New York, 1963), p. 718.
39. R. C. WEAST (Ed.), "CRC Handbook of Chemistry and Physics", (CRC Press, Boca Raton, Florida, 1981) p. F-94.
40. R. FEDER, A. S. NOWICK and D. B. ROSENBLATT, *J. Appl. Phys.* **29** (1958) 984.
41. P. C. J. GALLAGHER, *Metall. Trans.* **1** (1970) 2429.
42. L. E. MURR, in "Interfacial Phenomena in Metals and Alloys" (Addison-Wesley, Reading, MA, 1975) p. 148.
43. T. S. KÊ, *J. Appl. Phys.* **19** (1948) 285.
44. P. YAVARI and T. G. LANGDON, *Acta Metall.* **30** (1982) 2181.
45. C. KITTEL, in "Introduction to Solid State Physics", 5th Edn (Wiley, New York, 1976) p. 100.
46. W. D. NIX and B. ILSCHNER, in "Strength of Metals and Alloys (ICSMA 5)", edited by P. Hansen, V. Gerold and G. Kostorz (Pergamon Press, Oxford, 1980) p. 1503.
47. R. RESNICK and R. W. BALLUFFI, *Trans. AIME* **203** (1955) 1004.
48. J. HINO, C. TOMIZUKA and C. WERT, *Acta Metall.* **5** (1957) 41.
49. K. J. ANUSAVICE and R. T. DEHOFF, *Metall. Trans.* **30** (1972) 1279.
50. J. C. FISHER, J. H. HOLLOMON and D. TURNBULL, *Trans. AIME* **175** (1948) 202.
51. F. A. MOHAMED and T. G. LANGDON, *Acta Metall.* **22** (1974) 779.
52. R. FUENTES-SAMANIEGO, W. D. NIX and G. M. POUND, *Phil. Mag.* **A42** (1980) 591.
53. R. FUENTES-SAMANIEGO and W. D. NIX, *Scripta Metall.* **15** (1981) 15.
54. R. FUENTES-SAMANIEGO, W. D. NIX and G. M. POUND, *Acta Metall.* **29** (1981) 487.

Received 5 June
and accepted 26 June 1990